Sheikh, Muhammad Usman; Ali, Muhsin; Carpintero, Guillermo; Ruttik, Kalle; Mutafungwa, Edward; Jantti, Riku

Channel Characterization at Sub-THz Band with Measurements and Ray Tracing in Indoor Case

Published in:
37th International Conference on Information Networking, ICOIN 2023

DOI:
10.1109/ICOIN56518.2023.10048904

Published: 22/02/2023

Document Version
Peer-reviewed accepted author manuscript, also known as Final accepted manuscript or Post-print

Please cite the original version:
Sheikh, M. U., Ali, M., Carpintero, G., Ruttik, K., Mutafungwa, E., & Jantti, R. (2023). Channel Characterization at Sub-THz Band with Measurements and Ray Tracing in Indoor Case. In *37th International Conference on Information Networking, ICOIN 2023* (pp. 178-183). (International Conference on Information Networking; Vol. 2023-January). IEEE. https://doi.org/10.1109/ICOIN56518.2023.10048904

Channel Characterization at Sub-THz Band with Measurements and Ray Tracing in Indoor Case

Muhammad Usman Sheikh*†, Muhsin Ali‡, Guillermo Carpintero‡, Kalle Ruttik*,
Edward Mutafangwa*, and Riku Jäntti*
*Department of Communications and Networking, Aalto University, 02150 Espoo, Finland
Email: {muhammad.sheikh, kalle.ruttik, edward.mutafangwa, riku.jantti}@aalto.fi
†Nokia Networks, Nokia, Finland
‡Universidad Carlos III de Madrid, 28911 Leganés, Spain
Email: {muali, guiller}@ing.uc3m.es

***Abstract*—Ultra-wide bandwidth (BW) available at terahertz (THz) and sub-THz frequencies makes these bands interesting for wireless communication systems. A large BW at the sub-THz frequency band offers a promising solution for applications with short-range and high data rate requirements. Since the provision of high-speed computational systems, deterministic channel models have been extensively used for indoor field prediction and radio channel characterization, especially for high frequencies i.e., millimeter wave (mmWave) and sub-THz frequencies. We have developed an in-house built ray tracing (RT) tool, capable of characterizing a radio channel with good accuracy and precision. The aim of this paper is to validate the power angular spectrum (PAS) acquired through our RT tool with the measurement data at sub-THz frequencies of 90, 95, and 100 GHz, in both line-of-sight (LOS) and non-LOS (NLOS) University corridor environment. A photonics-based measurement setup with high accuracy is utilized for generating the sub-THz signal, and for acquiring the measurement data. In addition to the PAS, other channel metrics considered for the analysis through RT simulations are root mean square delay spread (RMS-DS) and RMS angular spread (RMS-AS) in an azimuth plane. The results presented in this paper show that our in-house built RT is capable of providing considerably good agreement between the measured and simulated PAS in both LOS and NLOS states.**

***Index Terms*—Measurements, simulations, power angular spectrum, ray tracing, terahertz, THz, sub-THz, indoor.**

I. Introduction

The frequency spectrum available at sub-6 GHz band can be considered a suitable choice for providing large coverage, and for supporting data rate of several $Gbps$. Whereas millimeter wave (mmWave), sub-terahertz (sub-THz), and THz band have ample free bandwidth (BW) and offer a solution for applications with short or medium range and massive data rate requirement [1]. Especially, the sub-THz frequency band around 90-100 GHz can be effectively used for wireless access in ultra-dense indoor small cell deployments e.g., in the living room, conference room, office corridor, data center, etc. To design an efficient and working system at sub-THz band, it is critically important to have a better understanding of the propagation mechanism at targeted frequency bands. Deterministic channel models such as ray tracing (RT) have been widely used for estimating the path loss, finding the coverage, and characterizing the radio propagation channel [2]–[4]. Ray tracing simulations have several advantages as it is comparatively easy and fast to generate accurate channel models with considerably less effort with RT than performing actual measurement [5]. Furthermore, RT offers more flexibility in terms of time and resources. However, a detailed and proper description of the environment, floor plan with fine details, and exact information about the position of the user, and furniture is required by the RT tool for accurate and precise prediction [6], [7]. In the case of an indoor environment with line-of-sight (LOS), the main propagation mechanisms are specular reflection, diffraction, and diffuse scattering [1]. In literature, most of the available studies are for LOS channels in a sub-THz band, and adequate research work is not done for non-LOS (NLOS) channels [5], [8], [9]. In our previous work, the focus of the study was the LOS scenario. However, in this research study, we aim to validate 3D RT simulation results acquired through an in-house built RT tool with the measurement data, especially in the NLOS indoor environment.

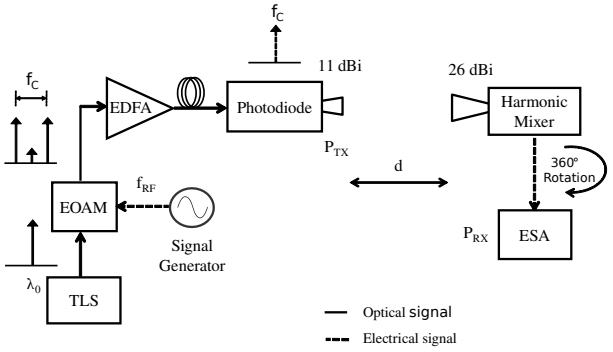

Fig. 1. Illustration of the measurement setup.

II. Measurement Setup and Scenario

Fig. 1 illustrates the measurement setup used for the generation and detection of the signal at considered sub-THz frequencies of 90, 95, and 100 GHz. A similar measurement setup is used in our previous work [9], where the focus was only on LOS cases. At the transmitter (TX) side, a photonics-based technique is employed for the generation of RF carrier wave frequency f_C. With such system it is easy to tune over a wide range of frequencies using the same set of

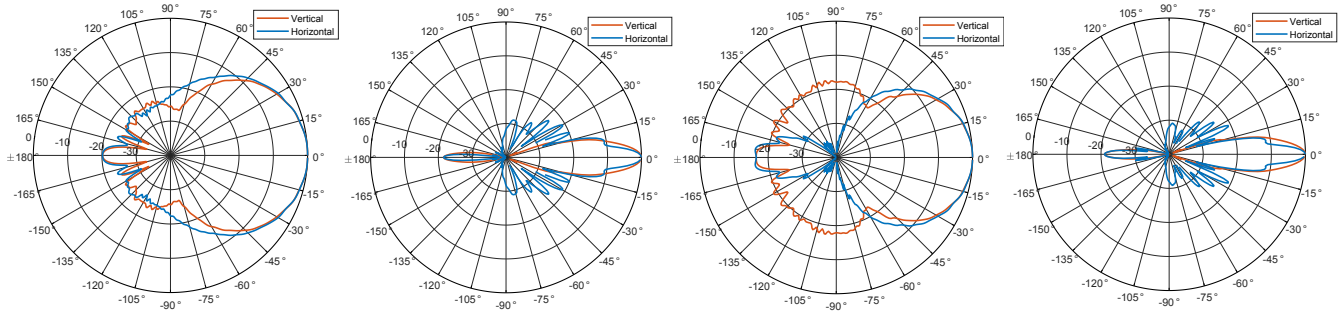

(a) (b) (c) (d)

Fig. 2. Radiation pattern of, (a) TX antenna at 90 GHz, (b) RX antenna at 90 GHz, (c) TX antenna at 100 GHz, (d) RX antenna at 100 GHz.

TABLE I
PARAMETERS OF TX AND RX ANTENNA.

	TX			RX		
	Max gain $[dBi]$	HPBW Vert $[^\circ]$	HPBW Horz $[^\circ]$	Max gain $[dBi]$	HPBW Horz $[^\circ]$	HPBW Horz $[^\circ]$
90 GHz	10.98	50.5	50	26.77	7.7	8.5
95 GHz	11.48	48	47.5	27.24	7.7	8.5
100 GHz	12.58	45.5	45	27.62	7.7	8.5

TABLE II
RECEIVER POSITIONS RELATIVE TO THE TRANSMITTER

Position	x [m]	y [m]	Distance [m]
P1	0	4.4	4.40
P2	0	7.2	7.20
P3	0	7.0	7.00
P4	2.4	6.7	7.17
P5	-1.4	6.7	6.82
P6	-2.1	6.7	7.02

components, and it offers the possibility to carry the RF signals over large distances. However, frequency tunability is difficult to achieve with conventional electronics. In conventional optical heterodyne technique, two free-running continuous-wave (CW) lasers are used, and therefore there is considerable frequency instability [10]. Whereas, in our measurement setup, the external modulation technique [11] is employed to stabilize the frequency of a carrier wave signal.

At the TX, a CW tunable laser source (TLS, Sacher Lasertechnik TEC-520-1550-030) operating at 1550nm band is used to generate an optical carrier λ_0, and that is then fed into a 50 GHz electro-optic amplitude modulator (EOAM). An external commercial signal generator (Keysight E8257D) is used for modulating an optical carrier λ_0 with an RF signal f_{RF}. The optical carrier λ_0 is suppressed by biasing the EOAM. The targeted carrier frequency f_C corresponds to the difference between the upper and lower sidebands i.e., $2f_{RF}$. With this technique of signal generation, the stability and the phase noise of the generated signal are directly related to that of the signal source. The signal f_C is amplified in an optical domain by an erbium-doped fiber amplifier (EDFA, Amonics AEDFA-PA-35-B-FA) and is carried over a 50m long optical fiber to the TX module in the corridor. The optical signal is converted into the RF domain by a PIN photodiode (U^2T XPDV4120R). The signal is radiated by a wide half-power beamwidth (HPBW) horn antenna (WR-10). The radiation pattern of the transmit antenna in azimuth and elevation planes changes considerably with the frequency of operation. For reference, the horizontal and vertical radiation pattern of the transmit antenna at 90 GHz and 100 GHz are shown in Fig. 2(a) and Fig. 2(c), respectively. Different parameters of the TX and RX antennas i.e., max gain, and the HPBW in the azimuth and elevation plane are given in Table I. A calibrated electronic harmonic mixer is used to accurately measure the generated RF power P_{TX} before transmission.

At the receiver side, a high-gain horn antenna (Anteral SGH-26-WR10) with narrow HPBW is used. The radiation pattern of the RX antenna in azimuth and elevation plane at 90 GHz and 100 GHz is shown in Fig. 2(b) and Fig. 2(d), respectively. The separation between the TX and RX module is denoted by d in Fig. 1. A harmonic mixing technique is used to detect the power P_{RX} at the receiver (RX) side. With the help of a commercial power-calibrated harmonic mixer (R&S FS-Z110) the received signal at f_C is down converted to an intermediate frequency. At the end, the received power is measured and recorded by the electrical spectrum analyzer (ESA, R&S FSW50). The RX module is rotated 360° by the automated motor in an azimuth plane to acquire PAS. whereas, the step size for rotating the stage 360° is set to 5°. Power angular spectrum measurements were conducted at the tee-junction of the University corridor, and the measurement environment from one side of the tee-junction is shown in Fig. 3(a). Whereas, a 3D model of the tee-junction of the University corridor is shown in Fig. 3(b). We have measured the PAS at six different positions. The locations of the TX and RX points are shown in Fig. 3(b). Positions P1-P3 are in LOS with the TX, whereas, the positions P4-P6 are located deep in the other corridor, and are in NLOS with the TX. The relative position of the RX points with respect to the TX, and the point-to-point distance between the TX and RX point is provided in Table II. The TX and RX antennas were 1m above the floor level. The RF front-end modules were synchronized and controlled from a remote location to ensure no physical interruption in the measurement environment.

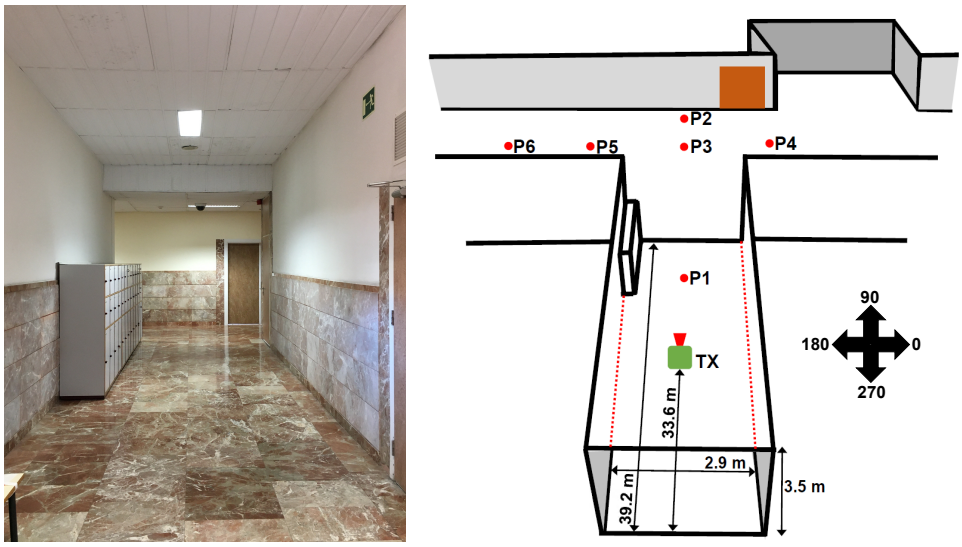

(a) (b)

Fig. 3. Measurement environment, (a) Actual, and (b) 3D model of a University corridor with TX and RX positions.

III. Simulation Methodology

This research work aims to validate an in-house built RT simulation tool by comparing the measurement data collected through PAS measurement with the simulation results acquired through RT simulations. For this purpose, a campaign of RT simulations was conducted for the measurement cases and scenarios discussed in Section II. To acquire realistic and definite RT simulation results, a 3D model of the tee-junction of the University corridor is used. A simulation environment was modeled with accurate geometry and dimension, and furniture like wooden closet and doors were included as shown in Fig. 3(b). The RT tool provides the information about ray paths between TX and RX point while considering the geometry of the environment and other objects. Our indigenous-built RT is able to capture LOS ray path along with ray paths with a given finite number of reflections, diffractions, and mix of reflections and diffractions, and paths with diffuse scattering from the walls. In addition to the reflected and diffracted ray paths from the walls, the RT simulation tool finds reflected paths from the ground and ceiling. Due to the considered high frequency of operation at sub-THz band i.e., 90-100 GHz, we have considered the ray paths up to two reflections and one diffraction only. Moreover, in the case of NLOS scenarios, due to high wall penetration loss at sub-THz frequencies, the penetrated paths through the walls of the corridor are not considered in our simulations. Furthermore, the general parameters e.g., transmission power, frequency of operation, azimuth, height, and downtilt of the TX and RX antennas, are set in the simulations as were used during the measurements. Subsequently, in the post-processing part of the simulation data, the impact of TX and RX antenna radiation patterns is considered. The radiation patterns of the TX and RX antennas in the azimuth and elevation domains were obtained from the manufacturers' data sheets.

IV. Results and Discussion

We have considered three radio channel characteristics i.e., power angular spectrum, root mean square delay spread (RMS-DS), and root mean square angular spread (RMS-AS), for this study. However, the measurement data is only available for the PAS, whereas, the RT simulation results are obtained for all three considered channel characteristics. As it can be seen in Fig. 3(b) that the receiver positions P1-P3 are in LOS, whereas, RX points P4-P6 are in NLOS with the TX. Therefore, the PAS of LOS and NLOS receiver points are analyzed separately. The RX position P1 is located at a distance of 4.4m from the TX, and Fig. 4(a-c) show the PAS of position P1 at 90, 95, and 100 GHz, respectively. In Fig. 4, the x-axis is the direction of arrival (DoA) at the receiver and that is expressed in degrees, and the y-axis is the received signal power in dBm. Maximum power is received while the RX antenna is directed towards 270° in an azimuth plane i.e., facing towards the transmit antenna. Both the measurement and simulation results show a strong reflected path coming from the back wall of the corridor at DoA of 90°. Not only in the direction of the LOS path but also in other directions, similar power levels were observed between the measured and simulated results at all three considered frequencies. In the case of position P2, the RX is located at a distance of 7.2m from the TX and is placed close to the back wall of the University corridor as shown in Fig. 3(b). It can be seen in Fig. 4(d-f) that maximum power is received in the direction of incoming LOS path i.e., 270°. However, in the case of P2, there exists a much stronger reflected path in the DoA of 90° as compared with P1. It should be noted, that the RT simulator quite accurately provides the received power level compared with measurement data in the direction of LOS, however, in case of strong reflection from the back wall, the received power level provided by the RT tool is slightly pessimistic. Similarly,

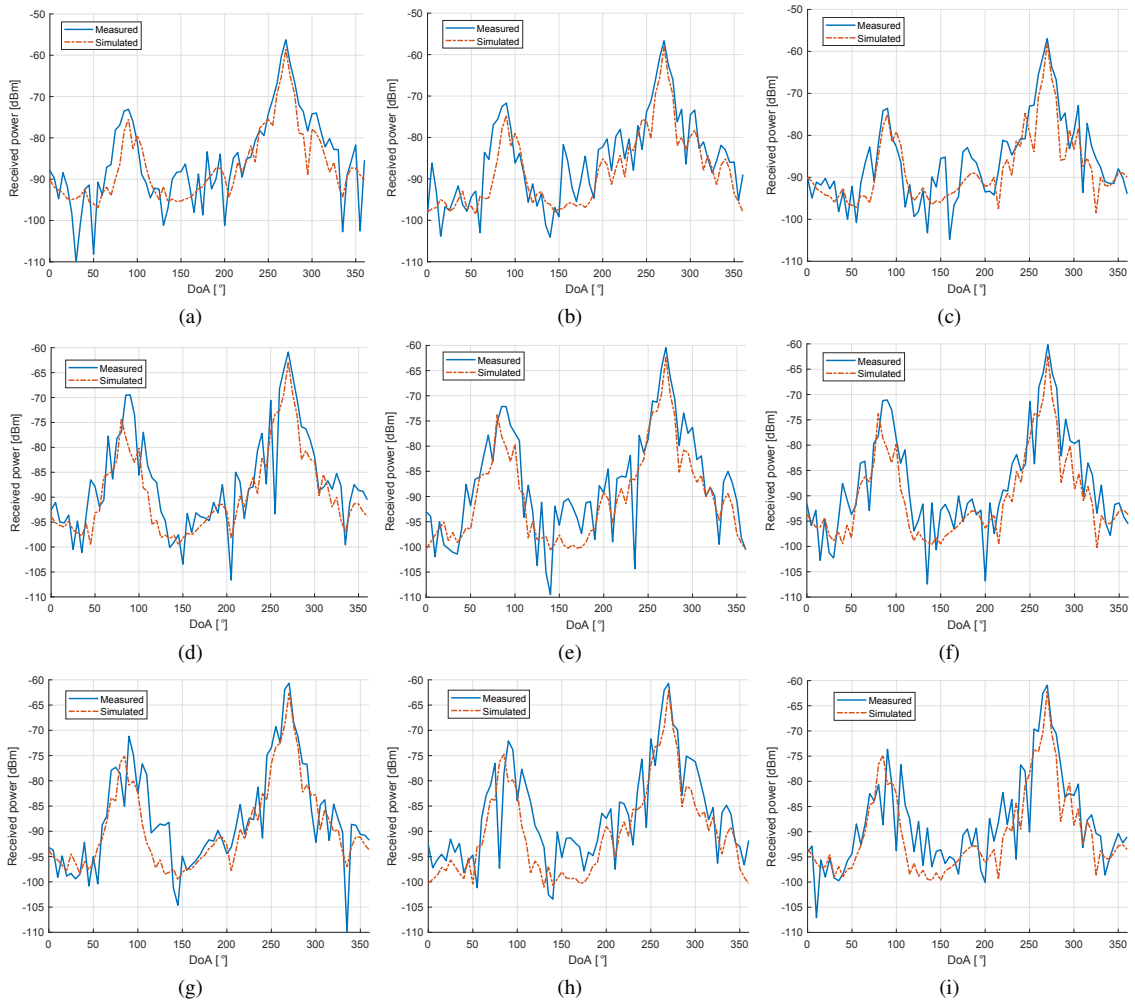

Fig. 4. Measured and simulated power angular spectrum of position, (a) P1 at 90 GHz, (b) P1 at 95 GHz, (c) P1 at 100 GHz, (d) P2 at 90 GHz, (e) P2 at 95 GHz, (f) P2 at 100 GHz, (g) P3 at 90 GHz, (h) P3 at 95 GHz, and (i) P3 at 100 GHz.

Fig. 4(g-i) provide PAS for position P3 at 90, 95, and 100 GHz, respectively, and P3 is located at a distance of 7m from the TX. Again, the PAS acquired through an in-house built RT tool is largely matched with the PAS obtained through measurements.

The receiver point P4 is in NLOS with TX and is located at a point-to-point distance of around 7.17m on the right side of the other corridor. Fig. 5(a-c) show the measured and simulated PAS for P4 at 90, 95, and 100 GHz, respectively. In this case, as the LOS path does not exist, both measurement and simulation data show that the strongest path reaching the P4 point is a reflected path from the door at a DoA of 100°. Whereas, the second peak found at 250° is due to the diffracted path from the corner of the corridor wall. The power of the diffracted path estimated by the RT tool is slightly pessimistic compared with the measured data. It should be noted that the distance between the TX and position P4 is almost same as between TX and P2. However, due to the absence of the LOS path, measured and simulation results show that there is a difference of around 12 dB between the maximum received power at P4 compared with P2.

Similarly, location point P5 is in NLOS and is located at a distance of around 6.82m on the left side of the corridor. It should be remembered that a wooden closet is placed around the corner of the corridor on the left side of the TX. Now, Fig. 5(d-f) show the measured and simulated PAS for P5 at 90, 95, and 100 GHz, respectively. Surprisingly, at three considered frequencies, the PAS obtained through simulations is found few dBs higher compared with the measurement data. It appears that the simulated PAS is having an offset of a few dBs with respect to the measured PAS. Later, it was found during the investigation of the measurement equipment and the measurement setup that the received power level degrades by a couple of dBs in the case of slightly twisted cables, as lower power is received at the photodetector. Therefore, it is assumed that in the case of measured PAS for P5, there exists some measurement error. This kind of problem highlights the sensitivity of the measurement equipment and points out the possibility of inducing errors in the measurement results due to human negligence. Otherwise, both measured and simulated PASs show that maximum power is received at a DoA of 80°

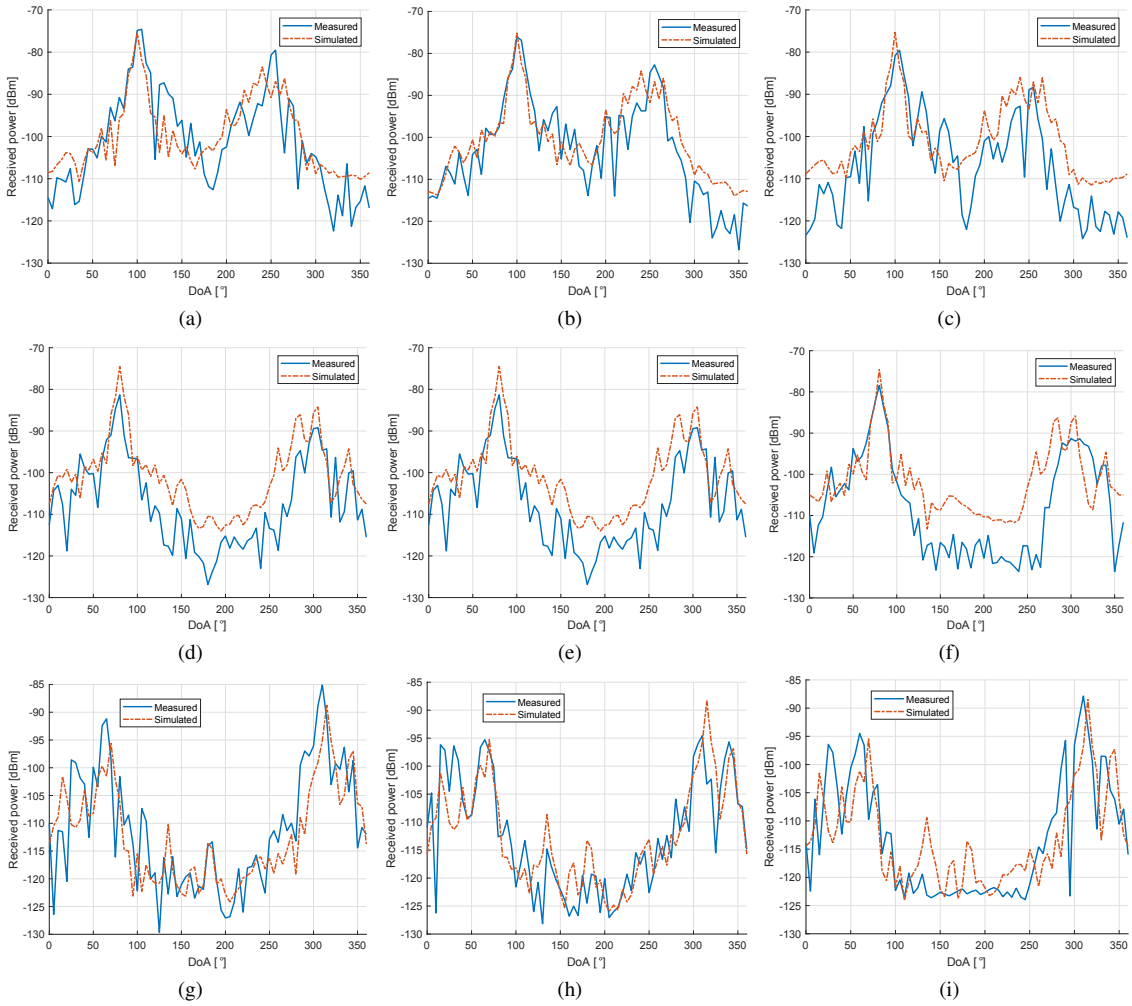

Fig. 5. Measured and simulated power angular spectrum of position, (a) P4 at 90 GHz, (b) P4 at 95 GHz, (c) P4 at 100 GHz, (d) P5 at 90 GHz, (e) P5 at 95 GHz, (f) P5 at 100 GHz, (g) P6 at 90 GHz, (h) P6 at 95 GHz, and (i) P6 at 100 GHz.

i.e., in the direction of the reflected path from the wall. Later, two small peaks around 285° and 305° are due to diffracted path around the corner and reflected path from the wall present on the left side of the TX, respectively. Interestingly, similar peaks are also captured by the measurement data at 95 GHz.

Subsequently, Fig. 5(g-i) show the measured and simulated PAS for P6, which is located at a distance of around 7.02m. It should be noted that the location point P6 is located a little deep in the corridor, such that a ray path with a single reflection cannot be reached. A mix of measurement results is achieved for P6, as in Fig. 5(g) the peak around 310° is due to the diffracted path from the corner of a wooden closet, and the peak around 70° is a mix of diffracted and reflected path. Whereas, in Fig. 5(h-i) a diffracted path from the other corner of the corridor around 340° is nicely captured by both measurements and simulations. Simulation results show that in the absence of LOS and paths single reflection, the maximum received power level is considerably attenuated i.e., around 14 dB, for P6 compared with P5, however, both are separated by a distance of just 0.7m. The results acquired through measurements and RT simulations presented in Fig. 4 and Fig. 5 show that our in-house built RT is able to provide reasonable accurate PAS in indoor corridor environment for RX points in both LOS and NLOS state, given a precise floor plan is provided.

Finally, Table III provides the measured and simulated received power, along with the RMS-DS and RMS-AS acquired through simulation, in the direction of the strongest incoming path. In the case of LOS, the strongest incoming path is the LOS path, whereas, in the case of NLOS condition, the strongest incoming path can be any of the reflected, diffracted, or path with a mix of them. It is found that the root mean square error (RMSE) between the measured and simulated received power level was limited to 2.6, 4.0, and 2.6 dB at 90, 95, and 100 GHz frequency of operation, respectively. It should be noted that this error includes the impact of the measurement error which is induced most probably due to the twisting of optical fiber as discussed earlier. It can be seen in Table III that the received power level is attenuated by roughly 12 dB when the RX point with similar distance move from LOS to

TABLE III
SUMMARY OF RESULTS

Pos	90 GHz				95 GHz				100 GHz			
	Meas RX pwr [dBm]	Sim RX pwr [dBm]	DS $[ns]$	AS $[^\circ]$	Meas RX pwr [dBm]	Sim RX pwr [dBm]	DS $[ns]$	AS $[^\circ]$	Meas RX pwr [dBm]	Sim RX pwr [dBm]	DS $[ns]$	AS $[^\circ]$
P1	-56.3	-58.6	3.1	1.7	-56.7	-58.1	3.1	1.9	-57.0	-58.0	3.3	1.9
P2	-60.9	-62.9	5.1	1.0	-60.5	-62.4	4.9	1.2	-60.2	-62.3	5.3	1.5
P3	-60.6	-62.6	4.9	0.6	-60.7	-62.1	4.7	1.3	-60.9	-62.1	5.2	1.1
P4	-74.9	-75.5	0.1	1.1	-76.1	-75.1	0.1	0.9	-79.6	-75.2	0.1	1.0
P5	-78.5	-74.9	0.1	1.1	-81.3	-74.5	0.1	0.8	-78.5	-74.6	0.1	0.8
P6	-85.1	-88.7	0.4	1.4	-94.6	-88.3	0.4	1.2	-87.9	-88.4	0.3	1.2

NLOS state i.e., by comparing P2 and P3 with P4. Similarly, the impact of the absence of a path with a single reflection can be seen by comparing the power levels of positions P5 and P6, as the received power level is further reduced by around 13 dB. Additionally, it should be noticed that for LOS location points i.e., P1-P3, the RMS-DS is considerably large compared with the NLOS points i.e., P4-P6, due to the multipath richness of the environment. Furthermore, RMS-DS mainly depends upon the geometry of the environment, therefore, for each RX point almost identical RMS-DS results are obtained for 90, 95, and 100 GHz frequency of operation. Table III shows that in a considered corridor environment and scenario, the maximum value of RMS-DS was limited to 5.3ns. Coherence bandwidth is inversely proportional to DS, therefore, 5.3ns of RMS-DS gives large coherence bandwidth. Similarly, due to the usage of an antenna with narrow HPBW in a horizontal plane at the receiver side, the RMS-AS was limited to $0.6 - 1.9^\circ$ range.

V. CONCLUSION

In this research work, a sophisticated and calibrated photonics-based measurement setup for sub-THz frequencies was used to measure PAS at six different static positions i.e., P1-P3 in LOS, and P4-P6 in NLOS, in an indoor University corridor environment. This paper further validated the PAS acquired through an in-house built RT tool with the measurement data at three targeted sub-THz frequencies i.e., 90, 95, and 100 GHz. Our own developed RT is capable of finding the LOS path along with other specular reflected paths, diffracted paths, paths with a mix of reflection and diffraction, diffused scattered paths, and paths with reflection from the ceiling and ground of the floor. The results presented in this paper show that our in-house built RT is able to provide reasonable accurate PAS in a LOS multipath-rich environment as well as in a NLOS condition. A fair agreement is found between the measured and simulated received PAS at three considered frequencies. This paper also highlighted the sensitivity of the measurement setup, as twisting of optical fiber can result in a decrease in received power level, and this type of human negligence adds error in the measurement data. The results presented in this paper show that in the direction of maximum received power the RMSE between the measured and simulated received power was limited to 2.6, 4.0, and 2.6 dB at 90, 95, and 100 GHz frequency of operation, respectively. Ray tracing simulations revealed that for LOS points the RMS-DS is considerably large i.e., $3.1 - 5.3$ns, compared with the NLOS points i.e., $0.1 - 0.4$ns, due to multipath richness of the environment. The RMS-AS in the azimuth plane depends on the horizontal HPBW of the antenna. Due to the usage of the antenna with a narrow HPBW at the receiver side, the RMS-AS was limited to $0.6 - 1.9^\circ$ range. In this work, only few static points were considered, however, in the future, we plan to use our RT tool for more complex and dynamic scenarios.

ACKNOWLEDGEMENT

This work has been partially supported by the TERAWAY project funded by the European Unions Horizon 2020 research and innovation programme under grant agreement No 871668.

REFERENCES

[1] S. Kim, W. T. Khan, A. Zajić, and J. Papapolymerou, "D-band channel measurements and characterization for indoor applications," *IEEE Transactions on Antennas and Propagation*, vol. 63, no. 7, pp. 3198–3207, 2015.

[2] J. Järveläinen, K. Haneda, and A. Karttunen, "Indoor propagation channel simulations at 60 ghz using point cloud data," *IEEE Transactions on Antennas and Propagation*, vol. 64, no. 10, pp. 4457–4467, 2016.

[3] S. Hur, S. Baek, B. Kim, J. Park, A. F. Molisch, K. Haneda, and M. Peter, "28 ghz channel modeling using 3d ray-tracing in urban environments," in *2015 9th European Conference on Antennas and Propagation (EuCAP)*, 2015, pp. 1–5.

[4] S. Soni and A. Bhattacharya, "An Efficient Two-Dimensional Ray-Tracing Algorithm For Modeling of Urban Microcellular Environments," *International Journal of Electronics and Communications*, vol. 66, no. 6, pp. 439 – 447, June. 2012.

[5] B. Peng, S. Rey, and T. Kürner, "Channel characteristics study for future indoor millimeter and submillimeter wireless communications," in *2016 10th European Conference on Antennas and Propagation (EuCAP)*, 2016, pp. 1–5.

[6] V. Degli-Esposti, F. Fuschini, E. M. Vitucci, M. Barbiroli, M. Zoli, L. Tian, X. Yin, D. A. Dupleich, R. Müller, C. Schneider, and R. S. Thomä, "Ray-tracing-based mm-wave beamforming assessment," *IEEE Access*, vol. 2, pp. 1314–1325, 2014.

[7] S. Priebe, M. Kannicht, M. Jacob, and T. Kürner, "Ultra broadband indoor channel measurements and calibrated ray tracing propagation modeling at thz frequencies," *Journal of Communications and Networks*, vol. 15, no. 6, pp. 547–558, 2013.

[8] K. Guan, B. Ai, D. He, F. Zhu, H. Yi, J. Dou, and Z. Zhong, "Channel sounding and ray tracing for thz channel characterization," in *2020 13th UK-Europe-China Workshop on Millimetre-Waves and Terahertz Technologies (UCMMT)*, 2020, pp. 1–3.

[9] M. U. Sheikh, M. Ali, G. Carpintero, K. Ruttik, E. Mutafangwa, and R. Jäntti, "Power angular measurements and ray tracing simulations at sub-thz frequencies in corridor," in *2022 IEEE Wireless Communications and Networking Conference (WCNC)*, 2022, pp. 1587–1592.

[10] T. Nagatsuma, S. Horiguchi, Y. Minamikata, Y. Yoshimizu, S. Hisatake, S. Kuwano, N. Yoshimoto, J. Terada, and H. Takahashi, "Terahertz wireless communications based on photonics technologies," *Opt. Express*, vol. 21, no. 20, pp. 23 736–23 747, Oct 2013.

[11] J. Yu, Z. Jia, L. Yi, Y. Su, G.-K. Chang, and T. Wang, "Optical millimeter-wave generation or up-conversion using external modulators," *IEEE Photonics Technology Letters*, vol. 18, no. 1, pp. 265–267, 2006.